PHYSICAL REVIEW C **87**, 055202 (2013)

Theoretical analysis of $\Lambda(1405) \to (\Sigma\pi)^0$ mass spectra produced in $p + p \to p + \Lambda(1405) + K^+$ reactions

Maryam Hassanvand,[1,2] Seyed Zafarollah Kalantari,[2] Yoshinori Akaishi,[1,3] and Toshimitsu Yamazaki[1,4]
[1]*RIKEN, Nishina Center, Wako, Saitama 351-0198, Japan*
[2]*Department of Physics, Isfahan University of Technology, Isfahan 84156-83111, Iran*
[3]*College of Science and Technology, Nihon University, Funabashi, Chiba 274-8501, Japan*
[4]*Department of Physics, University of Tokyo, Bunkyo-ku, Tokyo 113-0033, Japan*
(Received 30 October 2012; revised manuscript received 18 January 2013; published 8 May 2013)

We formulated the $\Lambda(1405)$ (abbreviated as Λ^*) $\to (\Sigma\pi)^0$ invariant-mass spectra produced in $p + p \to p + \Lambda^* + K^+$ reactions, in which both the incident channel for a quasibound K^-p state and its decay process to $(\Sigma\pi)^0$ were taken into account realistically. We calculated $M(\Sigma\pi)$ spectral shapes for various theoretical models for Λ^*. These asymmetric and skewed shapes were then compared with recent experimental data of HADES, yielding $M(\Lambda^*) = 1405^{+11}_{-9}$ MeV/c^2 and $\Gamma = 62 \pm 10$ MeV, where the interference effects of the $\bar{K}N$-$\Sigma\pi$ resonance with the $I = 0$ and 1 $\Sigma\pi$ continuum are considered. The nearly isotropic proton distribution observed in DISTO and HADES is ascribed to a short collision length in the production of Λ^*, which justifies the high sticking mechanism of Λ^* and the participating proton into K^-pp.

DOI: 10.1103/PhysRevC.87.055202 PACS number(s): 21.45.−v, 13.75.−n, 21.30.Fe, 21.90.+f

I. INTRODUCTION

The $\Lambda(1405)$ resonance discovered in 1961 [1] (called herein Λ^*) has strangeness $S = -1$, spin-parity $J^P = (\frac{1}{2})^-$, and isospin $I = 0$. It has been interpreted as a quasibound state of K^-p embedded in the $\Sigma + \pi$ continuum since Dalitz-Tuan's original prediction [2]. In recent years, Akaishi *et al.* derived phenomenologically a complex $\bar{K}N$ interaction (called here the *AY* interaction) [3–5] based on the mass and width of $\Lambda(1405)$, $M = 1405.1^{+1.3}_{-1.0}$ MeV/c^2 and $\Gamma = 50 \pm 2$ MeV [6–8] [the so-called $\Lambda(1405)$ ansatz]. They applied this very attractive interaction to few-nucleon systems involving one and two $\bar{K}$'s and found nuclear bound states with unusually high nuclear density [3,9–12]. On the other hand, a totally different framework with a double-pole structure of $\Lambda(1405)$ has emerged on the basis of chiral SU(3) dynamics (called here *Chiral*), on which $\Lambda(1405)$ is claimed to consist of two poles around 1420 and 1390 MeV/c^2, which are coupled mainly to $\bar{K}N$ and $\Sigma\pi$ channels, respectively [13,14]. Then, the resulting weakly attractive $\bar{K}N$ interaction leads to much shallower $\bar{K}$ bound states [15,16].

Thus, it is vitally important to determine the location of the K^-p resonance, whether $\Lambda(1405)$ is located at 1405 MeV/c^2 or above 1420 MeV/c^2, from experimental data without prejudice. For this purpose we have to treat the $\Lambda(1405)$ structure with the *AY* model and the *Chiral* model on equal footing to be compared with experimental data. To resolve this issue, observations of $M(\Sigma\pi)$ spectra associated with resonant formation of Λ^* in the stopped-K^- absorption in ^{3,4}He [17] and also in d [18] have been proposed. Whereas old bubble-chamber experiments of stopped K^- in ^{4}He [19] indicated a preference of $\Lambda(1405)$ over $\Lambda(1420)$ [8,18], a much more precise experiment with a deuteron target is expected at J-PARC [20]. Alternatively, Jido *et al.* [21] proposed an in-flight K^- reaction on d, whereas Miyagawa and Haidenbauer [22] questioned the effectiveness of this method. In any case, old data on the in-flight $K^- + d$ reaction by Braun *et al.* [23] had a large statistical uncertainty in distinguishing $\Lambda(1420)$ and $\Lambda(1405)$, according to our statistical analysis. Future experiments at J-PARC of both stopped-K^- [20] and in-flight K^- [24] on d are expected to give a convincing conclusion.

Recent experiments on high-energy pp collisions have produced important data on the production of $\Lambda(1405)$:

$$p + p \to p + \Lambda^* + K^+, \quad \Lambda^* \to \Sigma^{+,0,-} + \pi^{-,0,+}. \qquad (1)$$

The ANKE experiment at COSY with an incident kinetic energy (T_p) of 2.83 GeV by Zychor *et al.* [25] has yielded a $(\Sigma^0\pi^0)^0$ invariant-mass spectrum. It was analyzed by Geng and Oset [26] based on chiral SU(3) dynamics. They showed that the reaction in the Λ^* production region is dominated by the $|T_{21}|^2k_2$ process, and they claimed that the spectrum develops a pronounced strength around 1420 MeV/c^2, which differs from the 1405 MeV/c^2 peak in Hemingway's data [27] analyzed by the $|T_{22}|^2k_2$ process [6,7] (see also Akaishi *et al.* [28]). This result might have been accepted as evidence for a double-pole structure of Λ^* predicted by chiral SU(3) dynamics [13,14], if the statistics of the data were good enough. The ANKE data were also analyzed by Esmaili *et al.* [18], who, on the contrary, showed from a fair statistical comparison between the two models that the data were in more favor of the *AY* model, but the statistical significance was not sufficient to conclusively distinguish between *Chiral* and *AY* models. Thus, new data from HADES of GSI, which have just been published [29,30], are valuable for solving the present controversy.

In the present paper we formulate the spectral shape of the $(\Sigma\pi)^0$ mass to provide theoretical guides to analyze experimental data of $(\Sigma\pi)^0$ mass spectra from the above reaction. We take into account both the formation and the decay processes of $\Lambda(1405)$ in pp reactions realistically, following our $\bar{K}N - \Sigma\pi$ coupled-channel formalism [5]. In this way, we derive the general form of the spectral function, which is not symmetric but skewed with respect to the pole position.

Then, we analyze $(\Sigma^{+-}\pi^{-+})^0$ spectra from HADES at $T_p = 3.50$ GeV [30].

II. FORMULATION

A. Coupled-channel treatment of Λ^*

Our coupled-channel treatment of $\Lambda(1405)$ is described in [5,18]. We employ a set of separable potentials with a Yukawa-type form factor,

$$\langle \vec{k}_i'|v_{ij}|\vec{k}_j\rangle = g(\vec{k}_i')\, U_{ij}\, g(\vec{k}_j), \tag{2}$$

$$g(\vec{k}) = \frac{\Lambda^2}{\Lambda^2+\vec{k}^2}, \tag{3}$$

$$U_{ij} = \frac{1}{\pi^2}\frac{\hbar^2}{2\sqrt{\mu_i\mu_j}}\frac{1}{\Lambda}s_{ij}, \tag{4}$$

where i (j) stands for the $\bar{K}N$ channel, 1, or the $\pi\Sigma$ channel, 2, and μ_i (μ_j) is the reduced mass of channel i (j). Two of the nondimensional strength parameters, s_{11} and s_{12}, with a fixed s_{22} are adjusted so as to reproduce a set of assumed M and Γ values for the Λ^* pole [5]. The transition matrices,

$$\langle \vec{k}_i'|t_{ij}|\vec{k}_j\rangle = g(\vec{k}_i')\, T_{ij}\, g(\vec{k}_j), \tag{5}$$

satisfy

$$T_{ij} = U_{ij} + \sum_l U_{il}\, G_l\, T_{lj}, \tag{6}$$

$$G_l = \frac{2\mu_l}{\hbar^2}\int d\vec{q}\, g(\vec{q})\frac{1}{k_l^2-q^2+i\epsilon}\, g(\vec{q}). \tag{7}$$

The solution is given in a matrix form by

$$T = [1-UG]^{-1}U \tag{8}$$

with

$$(UG)_{lj} = -s_{lj}\sqrt{\frac{\mu_j}{\mu_l}}\frac{\Lambda^2}{(\Lambda-i\,k_j)^2}, \tag{9}$$

where k_j is a relative momentum in channel j.

Among the matrix elements, T_{11}, T_{12}, T_{21}, and T_{22}, the experimentally observable quantities below the $\bar{K}+N$ threshold are $-(1/\pi)\,\mathrm{Im}\,T_{11}$, $|T_{21}|^2k_2$, and $|T_{22}|^2k_2$, where the second term with $g^2(k_2)\,g^2(k_1)$ is a $\Sigma\pi$ invariant-mass spectrum from the conversion process, $\bar{K}N \to \Sigma\pi$ (which we call the "T_{21} invariant mass"). The T_{21} invariant mass coincides with the $\bar{K}N$ missing-mass spectrum in the mass region below the $\bar{K}+N$ threshold, as denoted by relation [18], that

$$\mathrm{Im}\,T_{11} = |T_{21}|^2\,\mathrm{Im}\,G_2. \tag{10}$$

The third term with $g^4(k_2)$ is a $\Sigma\pi$ invariant-mass spectrum from the scattering process, $\Sigma\pi \longrightarrow \Sigma\pi$ (which we call the "T_{22} invariant mass").

B. $\Lambda^* \to (\Sigma\pi)^0$ spectrum shape

The diagram for the reaction Eq. (1) is shown in Fig. 1. The decay processes via T_{21} and T_{22} are also given in this figure. The kinematical variables in the c.m. of the pp collision for both the formation and the decay processes are given in Fig. 2.

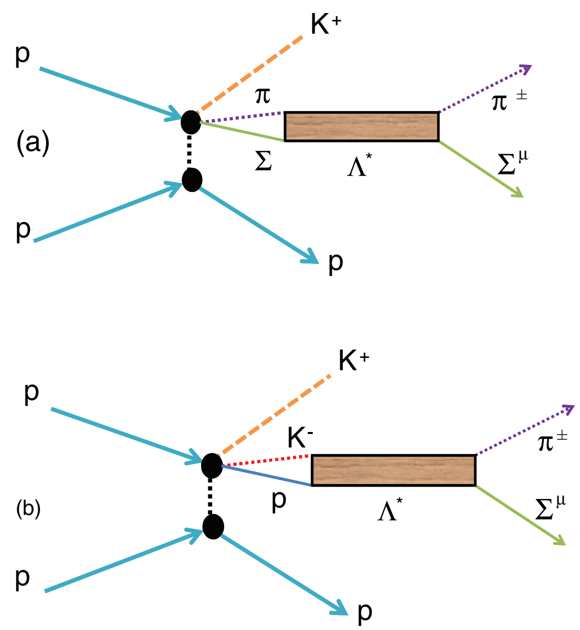

FIG. 1. (Color online) Feynman diagrams for the $p+p \to p+K^+ + \Lambda^* \to p+K^+ + (\Sigma\pi)^0$ reaction for (a) the process via T_{22} and (b) the process via T_{21}.

In the present reaction we use $|T_{21}|^2k_2$ because the incident channel to bring $\Lambda(1405)$ is K^-+p together with K^+ [see Fig. 1(b)]. This was also concluded by Geng and Oset [26], who studied the reaction mechanism in detail. The $|T_{22}|^2k_2$ spectrum would be applicable when Σ and π mesons are available in the incident channel, as shown in Fig. 1(a). The $|T_{22}|^2k_2$ spectrum is characterized by a large tail [18] in the higher-mass region up to the kinematical limit, which can in principle be recognizable by an observed spectrum. Experimentally, however, a bump in the upper-tail region

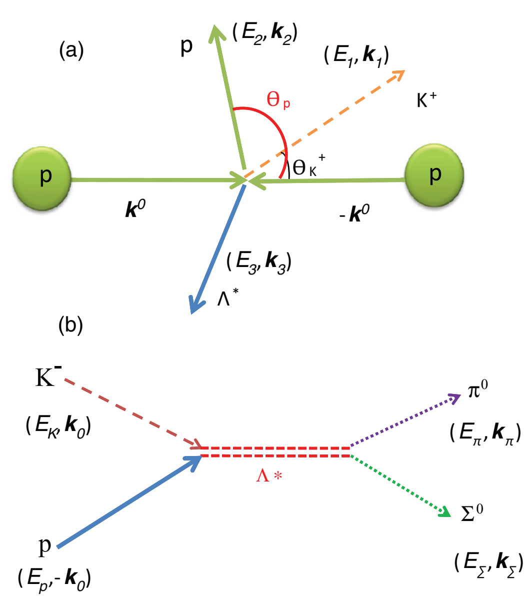

FIG. 2. (Color online) Kinematical variables in the center of mass of the pp collision for (a) the formation process, W_{form}, and (b) the decay channel, $G(x)$.

may be masked by an ambiguous shape of the continuous background and may thus be difficult to extract. We may allow a small admixture of $|T_{22}|^2 k_2$ in our likelihood analysis of the experimental data.

The $|T_{21}|^2 k_2$ and $|T_{22}|^2 k_2$ curves of the *Chiral* model, as given by Hyodo and Weise [15] as well as those of the *AY* model, are shown in Fig. 1 (upper) of Ref. [18]. They will be compared with the new HADES data at the end of the present paper.

C. Spectral function in the pp reaction: $S(x)$

Now, we consider the spectrum function of the invariant mass, $S(x)$, in the case of pp reactions. We compose it in the impulse approximation framework by using the incident channel function, $W_{\rm form}(x)$, and the decay channel one, $G(x)$, as follows:

$$S(x) = W_{\rm form}(x) \times G(x), \tag{11}$$

with

$$x = M(\Sigma\pi). \tag{12}$$

$G(x)$ is expressed in terms of the T matrices, T_{22} and T_{21}, as shown in Figs. 1(a) and 1(b). Each function calculated for an assumed M of the Λ^* pole is shown in Fig. 3.

D. Formation process function: $W_{\rm form}$

The Λ^* formation from pp collision is calculated in a similar way as was done in [4]. We apply an impulse approximation to the formation process of Fig. 1 with a model impulse t matrix,

$$\begin{aligned}
&\langle \vec{r}_{\Lambda^*-p}, \vec{r}_{(\Lambda^* p)-K^+} | t | \vec{r}_{p-p} \rangle \\
&\quad = T_0 \delta(\vec{r}_{\Lambda^*-K^+}) \int d\vec{r}\, \frac{\exp(-r/b)}{b^2 r} \delta(\vec{r}_{\Lambda^*-p} - \vec{r}) \delta(\vec{r}_{p-p} - \vec{r}),
\end{aligned} \tag{13}$$

where $\vec{r}_{a-b} = \vec{r}_a - \vec{r}_b$, T_0 is a strength parameter, and $b = m_B c/\hbar$ is a range which affects the dependence of the reaction amplitude on the momentum transfer to the adjacent proton in the $pp \to K^+ \Lambda^* p$ process. Then, the Λ^* formation probability is given as follows:

$$\begin{aligned}
W_{\rm form}(x) = {} & \frac{2|T_0|^2}{(2\pi)^3 (\hbar c)^6} \frac{E_0}{k_0} \int dE_1 \int d\Omega_1\, d\Omega_2 \left(\frac{1}{1 + b^2 Q^2} \right)^2 \\
& \times k_1 k_2 E_1 E_2 \left[1 + \frac{E_2}{E_3} \left(1 + \frac{k_1}{k_2} \cos(\theta_{pK^+}) \right) \right]^{-1},
\end{aligned} \tag{14}$$

where E_0 and k_0 are the initial energy and momentum in the c.m. frame, as given by

$$k_0 = \frac{1}{\hbar} \left[\frac{1}{2} M_p T_p \right]^{\frac{1}{2}}. \tag{15}$$

The other quantities, k_2, E_2, and E_3, become functions of x due to conservation of momentum and energy, which is applied to all the participating particles to take recoil effects into account.

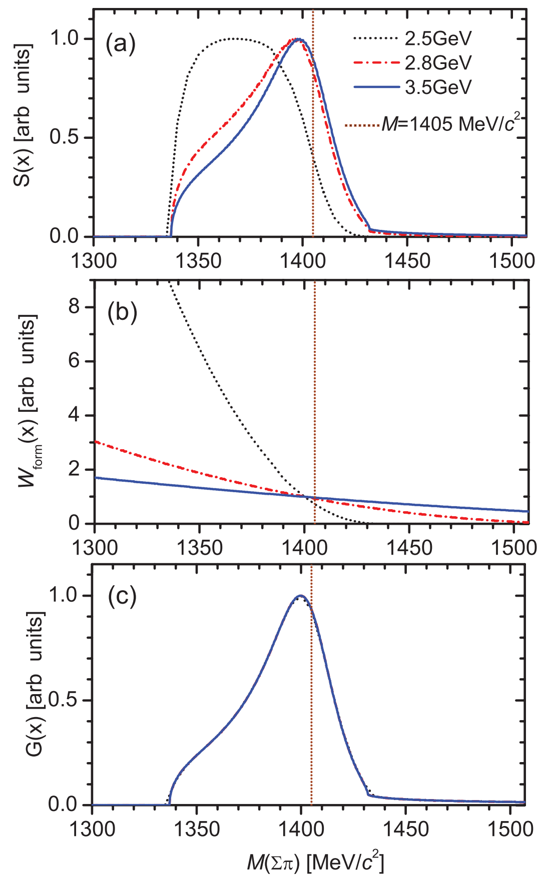

FIG. 3. (Color online) Normalized spectral functions $S(x)$ (a) composed of the formation-process function $W_{\rm form}$ (b) and the decay-process function $G(x)$ (c) for $T_p = 2.50$, 2.85, and 3.50 GeV. $m_B = 770$ MeV/c^2 and $(\theta_p, \theta_{pK^+}) = (90^\circ, 180^\circ)$. The M value of Λ^* is assumed to be 1405 MeV/c^2, as indicated by the vertical dashed line.

Also, $\theta_{pK^+} = (\theta_p - \theta_{K^+})$ is the angle between K^+ and p, b is the range of the pp reaction, and the momentum transfer, Q, is

$$Q = \left[{k_0}^2 + {k_2}^2 - 2\, k_0\, k_2 \cos \theta_p \right]^{\frac{1}{2}}. \tag{16}$$

As can be seen from the factor $1/(1 + b^2 Q^2)^2$, a shorter range of b can effectively moderate the strong suppression due to a large momentum transfer, Q, in a high-energy pp collision.

Figure 3(b) shows the behavior of $W_{\rm form}(x)$ for $T_p = 2.50$, 2.83, and 3.50 GeV, the curves of which are normalized at $x = 1400$ MeV/c^2. They have respective kinematical upper limits, which make the mass distribution damp toward the kinematical limit. As a result, the observed spectrum shape, $S(x)$, changes, as demonstrated in Fig. 3(a), whereas $G(x)$ is independent of T_p.

E. Decay process function: $G(x)$

The decay rate of $\Lambda(1405)$ to $(\Sigma\pi)^0$ is calculated by taking into account the emitted Σ and π particles realistically, following the generalized optical potential formalism in Feshbach theory [31], given by Akaishi *et al.* [5,28]. The decay function, $G(x)$, is not simply a Lorentzian but is skewed because the kinematic freedom of the decay particles is limited, particularly, when the incident proton energy, T_p, decreases and approaches the production threshold. Its general form is given as

$$G(x) = \frac{2(2\pi)^5}{\hbar^2 c^2} \frac{E_\pi E_\Sigma}{E_\pi + E_\Sigma} \mathrm{Re}\,[\tilde{k}(x)] |\langle \tilde{k}(x)|t|\tilde{k}_0(x)\rangle|^2, \quad (17)$$

where the relative momenta in the entrance and exit channels of Fig. 2(b) are calculated by

$$\tilde{k}_0(x) = \frac{c\sqrt{\lambda(x, m_K, M_p)}}{2\hbar\, x} \quad (18)$$

and

$$\tilde{k}(x) = \frac{c\sqrt{\lambda(x, m_\pi, M_\Sigma)}}{2\hbar\, x} \quad (19)$$

with

$$\lambda(x, m_1, m_2) \equiv (x + m_1 + m_2)(x + m_1 - m_2) \times (x - m_1 + m_2)(x - m_1 - m_2). \quad (20)$$

It should be noticed that $\lambda(x, m_K, M_p)$ becomes negative at around $x = 1400$ MeV$/c^2$, where we must choose a positive Im $\tilde{k}$ on the physical Riemann sheet. This case corresponds to direct excitation of the Λ^* quasibound state from the $p + p$ channel.

In the case of *AY*, the T matrix is

$$\langle \tilde{k}|t_{21}|\tilde{k}_0\rangle = g(\tilde{k})\, T_{21}\, g(\tilde{k}_0) \quad (21)$$

for the T_{21} process and

$$g(\tilde{k}) = \frac{\Lambda^2}{\Lambda^2 + \tilde{k}^2} \quad (22)$$

with $\Lambda = m'_B c/\hbar$, m'_B being the mass of an exchanged boson, and $\tilde{k}$ is the relative momentum of Σ and π.

The shape of $G(x)$, as given by Eq. (17), includes the momenta $\tilde{k}_0$ and $\tilde{k}$, which are functions of T_p. However, the function $G(x)$ is shown to depend only on the invariant-mass x; namely, $G(x)$ is a unique function of x and does not depend on T_p. It is bounded by the lower end ($M_l = M_\Sigma + m_\pi = 1328$ MeV$/c^2$) and the upper end ($M_u = M_p + m_{K^-} = 1432$ MeV$/c^2$).

It is to be noted that the position of the peak in $G(x)$ is significantly lower than the position of the pole ($M = 1405$ MeV$/c^2$) in T_{21}, as assumed here and indicated by the vertical dashed line. Furthermore, the position of the peak (or centroid) of $S(x)$ is lowered due to the formation channel function $W_{\mathrm{form}}(x)$.

III. NUMERICAL RESULTS

In this section we present results from numerical calculations, and we discuss their physical implications. The importance of the present work is to consider both $W_{\mathrm{form}}(x)$ and $G(x)$ functions. In most illustrative samples, we applied the *AY* model with the Particle Data Group (PDG) parameters of [7], $M = 1407$ MeV$/c^2$ and $\Gamma = 50$ MeV. To compare the *Chiral* model with the *AY* model on equal footing, we also applied the same procedure as above to Hyodo-Weise's T matrices to obtain realistic spectrum shapes $S(x)$.

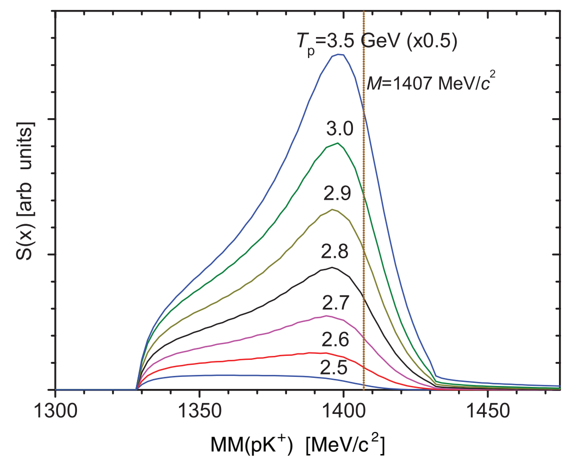

FIG. 4. (Color online) Incident energy dependence of the absolute values of the spectral function at $m_B = 770$ MeV$/c^2$ and $(\theta_p, \theta_{pK^+}) = (90^\circ, 180^\circ)$.

A. Dependence on the incident energy, T_p

For Eqs. (11), (14), and (17) again, it is clear that the spectral function depends on the incident proton energy due to the $W_{\mathrm{form}}(x)$ function and $G(x)$. Figure 4 shows absolute values of spectral functions $S(x)$ for various incident energies (T_p) at $m_B = 770$ MeV$/c^2$ and $(\theta_p, \theta_{pK^+}) = (90^\circ, 180^\circ)$. The shape of $S(x)$ is nearly the same, but toward the reaction threshold ($T_p^{\mathrm{thresh}} = 2.42$ GeV) not only does the absolute value diminish but also the spectral shape changes drastically, as shown in Fig. 3(a) for the normalized spectral functions at $T_p = 3.50$, 2.83, and 2.50 GeV. The most extreme case is seen at $T_p = 2.50$ GeV, where the main part of $x > 1400$ MeV$/c^2$ is missing due to the kinematical constraint, and a very skewed component below 1400 MeV$/c^2$ appears.

B. Behavior near the production threshold of T_p

The above prediction is indeed in good agreement with the observed spectra of DISTO at $T_p = 2.50$ and 2.85 GeV [33], as shown in Fig. 5. Even in such a very skewed spectrum, one can extract the decay function, $G(x)$, from an observed spectral function by taking the ratio

$$\mathrm{DEV}[G(x)] \equiv \frac{S(x)^{\mathrm{obs}}}{W_{\mathrm{form}}(x)} \quad (23)$$

using a calculated W_{form} function. This is a kind of the *deviation spectrum method* introduced in stopped-K^- spectroscopy [18].

C. Angular distribution and correlation

The cross section of this reaction has substantial angular dependence (Fig. 6), but the bound-state peak is distinct at any angle, and we can choose $(\theta_p, \theta_{pK^+}) = (90^\circ, 180^\circ)$, because the cross section is modest and the peak-to-background ratio

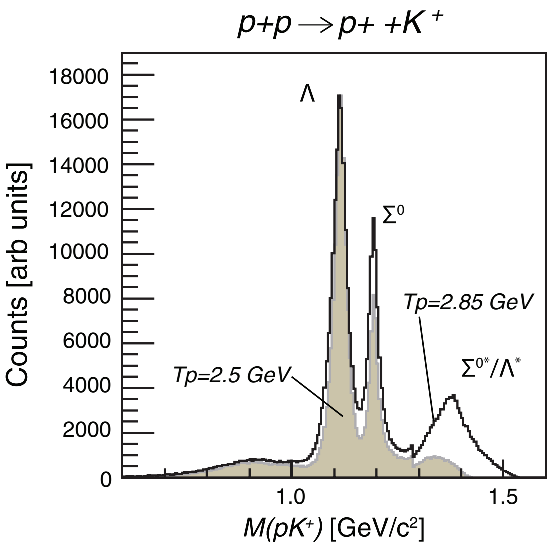

FIG. 5. (Color online) Experimental spectra of $\Delta M(pK^+)$ in the $pp \to p\Lambda K^+$ reaction at $T_p = 2.50$ and 2.85 GeV in DISTO experiments. Taken from [33].

remains large. The normalized cross sections (spectral shapes) at various angles are found to be nearly the same. Since the two incident protons are indistinguishable, the $\Lambda(1405)$ formation process is angular symmetric, as shown in Fig. 6. We can write

$$\sigma(\theta_p, \theta_{pK^+}) = \sigma(\pi - \theta_p, -\theta_{pK^+}) \tag{24}$$

for $\theta_p = 0^\circ$–90° and $\theta_{pK^+} = 0^\circ$–180°.

According to Eqs. (14) and (16), $W_{\rm form}$, and thus the spectral function, $S(x)$, are related to the outgoing proton angle, θ_p, and the angle between the outgoing proton and K^+, θ_{pK^+}, as shown in Fig. 7. Although these curves look different, the spectrum shape does not depend on the angle. We choose and use $\theta_p = 90^\circ$, $\theta_{pK^+} = 180^\circ$ in all of the following calculations.

D. Dependence on the exchanged boson mass

Figure 6 shows the normalized angular distributions of the outgoing proton, θ_p, for various masses of the exchanged

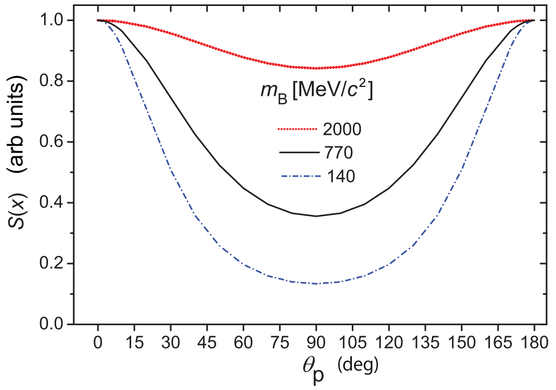

FIG. 6. (Color online) Normalized angular distributions of the outgoing proton for different exchanged boson masses, $m_B = 2000$, 770, and 140 MeV$/c^2$, at $T_p = 3.50$ GeV.

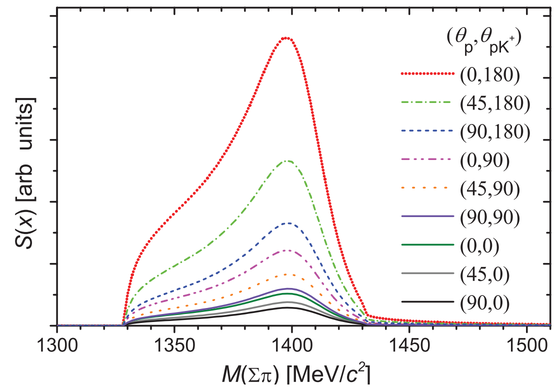

FIG. 7. (Color online) The spectral functions for various angles, $(\theta_p, \theta_{pK^+})$, for $T_p = 3.50$ GeV and $m_B = 770$ MeV$/c^2$.

boson, $m_B = 2000$, 770, and 140 MeV$/c^2$, at $T_p = 3.50$ GeV. The nearly isotropic angular distribution with a large boson mass explains the experimental data of HADES at $T_p = 3.50$ GeV [29,30], which shows that the proton angular distributions together with $\Lambda(1405)$ and $\Lambda(1520)$ are nearly isotropic. A similar behavior is observed in the DISTO data at $T_p = 2.85$ GeV (see Fig. 5 of the present paper and Refs. [33,34]). Such a short collision length as revealed in the production of $\Lambda(1405)$ in the pp reaction is one of the key mechanisms (Λ^* doorway) responsible for forming K^-pp from high sticking of Λ^* and p [4]. On the other hand, it is well known that the proton emitted in the ordinary $pp \to p + \Lambda + K^+$ reaction has sharp forward and backward distributions, indicating that the mediating boson is $m_B = m_\pi$ [32–34].

IV. χ^2 FITTING OF HADES DATA

A. HADES data

In this section we analyze the recent HADES data for charged final states of $\Sigma^-\pi^+$ and $\Sigma^+\pi^-$ in a pp collision at $T_p = 3.50$ GeV. The data we use are the missing-mass spectra, $MM(pK^+)$, deduced by the HADES group, as given in Fig. 1 of [30], which are corrected for acceptance and efficiency of the detector system. They are expressed as

$$Y(x) = Y_{\Lambda^*}(x) + Y_{\Sigma^*}(x) + Y_{\Lambda 1520}(x) + Y_{\rm NonRes}(x), \tag{25}$$

with Y_{Λ^*} for Λ^*, Y_{Σ^*} for $\Sigma(1385)$, $Y_{\Lambda 1520}$ for $\Lambda(1520)$, and $Y_{\rm NonRes}$ for the nonresonant continuum. The HADES group decomposed the experimental data, $Y(x)$, by the above four components, which were obtained by model simulations, among which the $\Sigma(1385)$ and the $\Lambda(1520)$ components were determined by using the experimental data. The shape of the nonresonant $\Sigma\pi$ continuum was simulated. In their fitting they cautiously excluded the area around 1400 MeV$/c^2$ for $MM(pK^+)$ in order not to bias the finally extracted shape of the Λ^* resonance. Then, they found that a simulation of the Λ^* region by using a relativistic s-wave Breit-Wigner distribution with a width of 50 MeV$/c^2$ and a pole mass of 1385 MeV$/c^2$ can reproduce the experimental data very well, but using instead the nominal mass of 1405 MeV$/c^2$ fails.

This conclusion depends on their assumption of the symmetric Breit-Wigner shape, which is not valid in the case of a broad resonance with adjacent endpoints, $M(\Sigma + \pi)$ and $M(p + K^-)$, as we have seen. Thus, in turn, we decided to set up an excess component, $Y_{\Lambda^*}(x)$, by subtracting the given three components from the experimental spectrum $Y(x)$ as

$$Y_{\Lambda^*}(x) = Y(x) - Y_{\Sigma^*}(x) - Y_{\Lambda 1520}(x) - Y_{\mathrm{NonRes}}(x), \quad (26)$$

where the statistical errors of $Y(x)$ are inherited to $Y_{\Lambda^*}(x)$.

B. Interference effects between the $\bar{K}N$ resonance and the $\Sigma\pi$ continuum

Before going into the analysis of the HADES data we discuss possible interference effects between the $\bar{K}N$ resonance and the $\Sigma\pi$ continuum.

1. Interference with the $I = 1$ $\Sigma\pi$ continuum

The charge-basis T matrices are related to the isospin-basis T matrices as

$$|T_{\Sigma^+\pi^-}|^2 \approx \frac{1}{3}|T_{I=0}|^2 + \frac{1}{2}|T_{I=1}|^2 + \sqrt{\frac{2}{3}}|T_{I=0}T_{I=1}|, \quad (27)$$

$$|T_{\Sigma^-\pi^+}|^2 \approx \frac{1}{3}|T_{I=0}|^2 + \frac{1}{2}|T_{I=1}|^2 - \sqrt{\frac{2}{3}}|T_{I=0}T_{I=1}|, \quad (28)$$

where $|T_{I=2}|^2$ is neglected. The HADES $\Sigma^+\pi^-$ and $\Sigma^-\pi^+$ data show similar behavior: the χ^2 best-fit mass of each of the two spectra is obtained to be very close to one another. This means that the interference term between $I = 0$ and $I = 1$ has only a small effect on the resonance spectral shape. Then, we can treat the $I = 1$ contribution as a part of Y_{NonRes} in the analysis of the $I = 0$ Λ^* resonance, disregarding the interference especially for the sum of the $\Sigma^+\pi^-$ and $\Sigma^-\pi^+$ data.

2. Interference with the $I = 0$ $\Sigma\pi$ continuum

$\Lambda(1405)$ $(=\Lambda^*)$ is an $I = 0$ $L = 0$ $\bar{K}N$ resonance state coupled with the $I = 0$ $L = 0$ $\Sigma\pi$ continuum. Our theoretical spectrum curves in Fig. 11 already include the $\bar{K}N$ threshold effect and also the interference effect with the $I = 0$ $L = 0$ $\Sigma\pi$ continuum, because we have solved a $\bar{K}N$-$\Sigma\pi$ coupled-channel T-matrix equation. Thanks to the separation of Y_{NonRes} by the HADES group we need not calculate contributions from the $I = 0$ $L \geqslant 1$ $\Sigma\pi$ continuum and $I = 1$ all L $\Sigma\pi$ continuum, which cause no interference to the $I = 0$ $L = 0$ Λ^* resonance and therefore can be treated as Y_{NonRes}: this is a great advantage of the HADES data for extracting the resonance-pole parameters, the mass and the width of Λ^*.

Now we estimate the effect of the $\bar{K}N$ threshold and the effect of interference with the $I = 0$ $L = 0$ $\Sigma\pi$ continuum. By fixing the mass of Λ^* to be 1405 MeV$/c^2$, we change AMY's interaction strengths, s_{11}, $s_{12} = s_{21}$, so as to reproduce a given width range of 10–70 MeV. The obtained mass spectra are discussed below.

Figure 8 shows the $\bar{K}N$ threshold effect on the $\Sigma\pi$ invariant mass spectrum, $|t_{21}|^2k_2$, where the interference effect

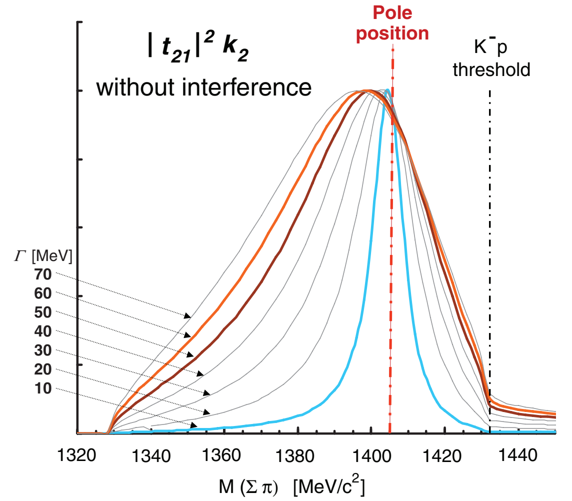

FIG. 8. (Color online) Transition mass spectrum, $|t_{21}|^2k_2$, including the $\bar{K}N$ threshold effect. All the heights are normalized to a same value.

is suppressed by putting $s_{22} = 0$. When the width is narrow enough, the spectrum is almost symmetric with a peak close to the pole position. When the width becomes wide, the peak position is lowered from the pole position and the spectrum shape is skewed: this is the $\bar{K}N$ threshold effect on the spectrum. Figure 9 shows results when the interference effect with the $I = 0$ $L = 0$ $\Sigma\pi$ continuum is switched on. The interference effect is not so large for the transition mass spectrum, $|t_{21}|^2k_2$, since the entrance channel to form Λ^* has no $\Sigma\pi$ continuum component.

On the other hand, Fig. 10 shows results of the conventional mass spectrum, $|t_{22}|^2k_2$, including the interference effect with the $I = 0$ $L = 0$ $\Sigma\pi$ continuum. The interference effect is rather large, since the entrance going to Λ^* consists of just $\Sigma\pi$ continuum components, which make the resonance shape

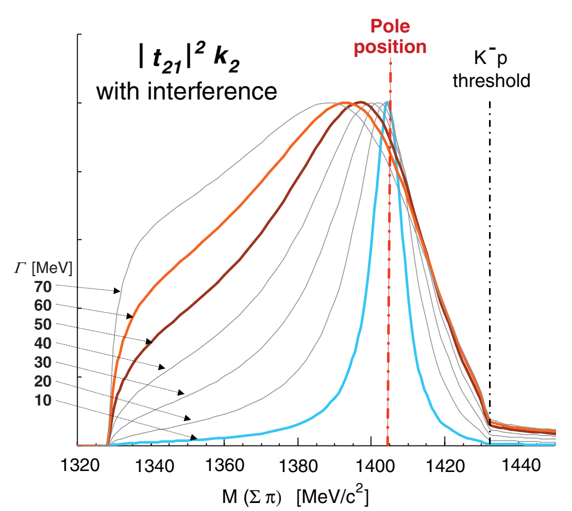

FIG. 9. (Color online) Transition mass spectrum, $|t_{21}|^2k_2$, including both the $\bar{K}N$ threshold effect and the interference effect with the $I = 0$ $L = 0$ $\Sigma\pi$ continuum. All the heights are normalized to a same value.

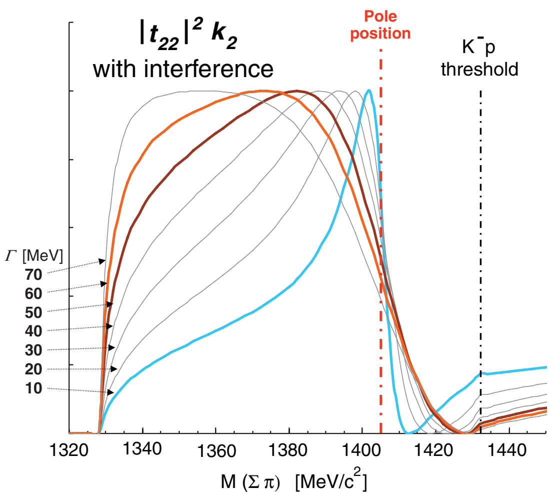

FIG. 10. (Color online) Conventional mass spectrum, $|t_{22}|^2 k_2$, including both the $\bar{K}N$ threshold effect and the interference effect with the $I = 0$ $L = 0$ $\Sigma\pi$ continuum. All the heights are normalized to a same value.

deform appreciably. The peak shift comes almost from the interference with the $I = 0$ $L = 0$ $\Sigma\pi$ continuum, as seen from an inflection at the pole position and a succeeding interference minimum (see Fig. 8(b) of [35]). The CLAS data [36] seem to be a case of $|t_{22}|^2 k_2$ where the coupling with the $\Sigma\pi$ continuum becomes significant. The interference between $I = 0$ and $I = 1$ $\Sigma\pi$ amplitudes gives rise to a strong charge dependence of $\Sigma^+\pi^-$, $\Sigma^0\pi^0$, and $\Sigma^-\pi^+$ mass spectra.

The HADES data are well fitted with the transition mass spectrum, $|t_{21}|^2 k_2$, as seen from the resemblance between $\Gamma = 60$ or 50 MeV curves of Fig. 9 and (a) or (b) of Fig. 11. It is noted that the peak shift takes place mainly due to the $\bar{K}N$ threshold effect in this case.

C. Deduced mass and width

The HADES spectra, as given in Fig. 1 of [30], indicate that the spectra of the two charged channels are similar to each other, yielding nearly the same M values. This fact indicates that the $\Sigma\pi$ resonance is formed by nearly pure charged states, $\Sigma^+\pi^-$ and $\Sigma^-\pi^+$, without isospin mixing. It also justifies the use of T_{21} for the analysis of $M(\Sigma\pi)$ in the case of pp reactions. On the other hand, the statistical fluctuation of each charged-channel spectrum is rather large. Thus, for the final analysis we use the sum data of HADES ($\Sigma^+\pi^- + \Sigma^-\pi^+$), which is presented in Fig. 1(c) of [30]. Keeping the last three components of Eq. (26) fixed, we fit the experimental data of $Y_{\Lambda^*}(x)$ with $n = 21$ data points in the range of 1300 to 1550 MeV/c^2 (closed points with error bars in Fig. 11) by assumed theoretical functions $S(x)$.

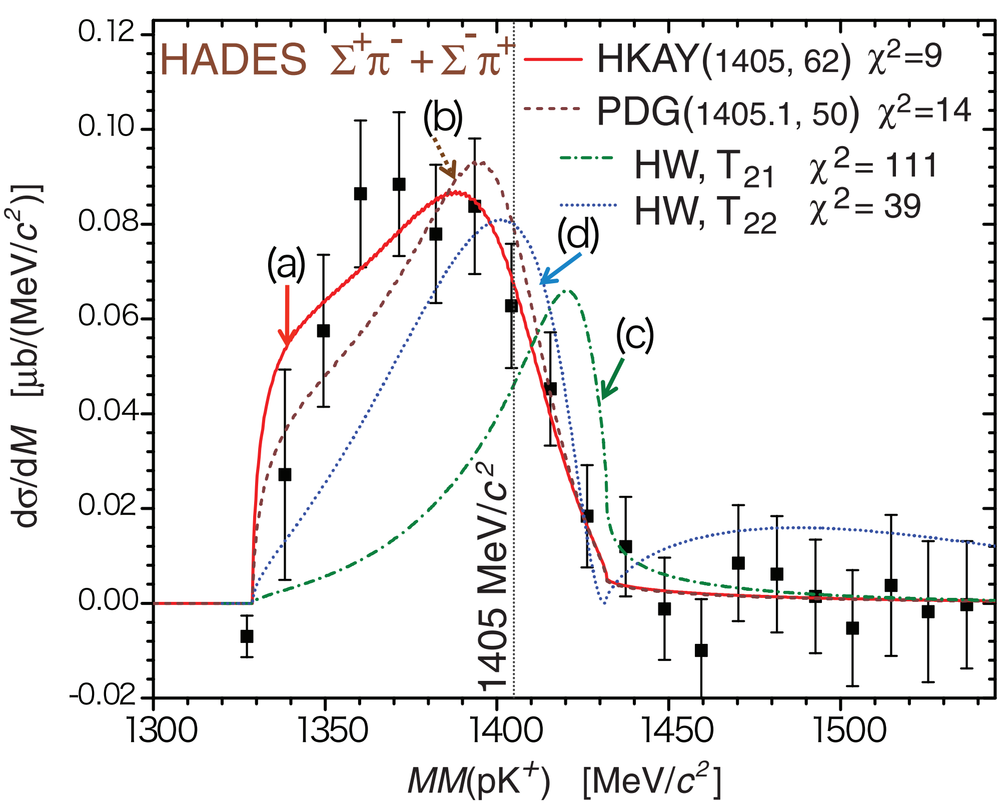

FIG. 11. (Color online) Comparison of HADES data ($\Sigma^+\pi^- + \Sigma^-\pi^+$, closed squares) at $T_p = 3.50$ GeV [30] with best-fit theoretical spectral functions $S(x)$. (a) Best-fit HKAY curves (with $\chi^2 = 9.5$, $M = 1405^{+11}_{-9}$ MeV/c^2, and $\Gamma = 62 \pm 10$ MeV). (b) *AY* model with the PDG parameters (with $\chi^2 = 14$, $M = 1405.1^{+1.3}_{-1.0}$ MeV/c^2, and $\Gamma = 50$ MeV [8]). The *Chiral* model using HW's T_{21} [with $\chi^2 = 111$, (c)] and T_{22} [with $\chi^2 = 39$, (d)].

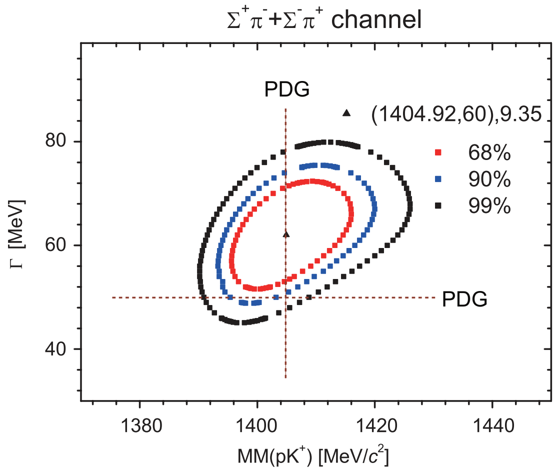

FIG. 12. (Color online) Confidence level contours from χ^2 fitting of the HADES data of $\Sigma^+\pi^- + \Sigma^-\pi^+$ at $T_p = 3.50$ GeV. The PDG values are also shown.

Generally, the experimental histogram, N_i, $i = 1, \ldots, n$, with respective statistical errors, σ_i, is fitted to a theoretical curve, $S(x; M, \Gamma)$, with $x = MM(pK^+)$ involving the mass M and width Γ as free parameters by minimizing the χ^2 value:

$$\chi^2(M, \Gamma) = \sum_{i=1}^{n} \left(\frac{N_i - S(x_i; M, \Gamma)}{\sigma_i} \right)^2. \quad (29)$$

Figure 11 shows the results of the χ^2 fitting, where the HADES data ($\Sigma^+\pi^- + \Sigma^-\pi^+$) at $T_p = 3.50$ GeV [30] are compared with best-fit theoretical spectral functions, $S(x)$. The present AY treatment (hereafter called HKAY), with the PDG values ($M = 1405.1^{+1.3}_{-1.0}$ MeV/c^2 and $\Gamma = 50$ MeV [8]) adopted, gives a remarkable fitting with $\chi^2 = 11$, which is comparable with the statistically expected value, $\langle \chi^2 \rangle_{\rm exp} \sim 19$. On the other hand, the *Chiral* model gives much larger χ^2 values of $\sim$111, when T_{21} is chosen, and of 39, when T_{22} is chosen. Another *Chiral* model spectrum by Geng and Oset [26] is almost identical to HW's T_{21}. Thus, the chiral models indicate a substantial deviation from the experimental data.

Furthermore, we can find best-fit values of (M, Γ) from drawing confidence contour curves by varying the parameters (M, Γ) in a plane. The results are shown in Fig. 12. From this contour mapping we obtain the following best-fit values with 68% confidence limits (1σ errors):

$$M = 1405^{+11}_{-9} \text{ MeV}/c^2, \quad (30)$$

$$\Gamma = 62 \pm 10 \text{ MeV}. \quad (31)$$

The best-fit curves are shown together with the experimental points in Fig. 11. The M value thus obtained from the present analysis of the new HADES data confirms the traditional value [7,8].

V. CONCLUDING REMARKS

We have presented results of our calculation for the spectral shape of $MM(pK^+)$ in the $pp \to p\Lambda^* K^+$ reaction based on the $\bar{K}N$-$\Sigma\pi$ coupled-channel treatment. We took into account both the entrance process and the decay process. The formation probability, $W_{\rm form}$, of Λ^* in a pp collision and the decay rate, $G(x)$, to $(\Sigma\pi)^0$ were formulated. The spectral function is given by $S(x) = W_{\rm form} \times G(x)$. It was found to be asymmetric and skewed due to the kinematic limitation imposed by the entrance channel. The peak of $S(x)$ is not located at the pole position.

With this tool in hand we analyzed the recent HADES data. The interference effects of the $\bar{K}N$-$\Sigma\pi$ resonance with the $I = 0$ and 1 $\Sigma\pi$ continuum are considered. Although the observed spectra of $MM(pK^+)$ appear to show the peak position at around 1385 MeV/c^2, the χ^2 fitting by our theoretical spectral functions provided $M = 1405^{+11}_{-9}$ MeV/c^2. This value is in good agreement with the values obtained from a recent analysis [17] of an old experimental data of stopped-K^- in ^{4}He [19], taken up as the updated PDG value ($M = 1405.1^{+1.3}_{-1.0}$ MeV/c^2) [8]. On the other hand, the *Chiral* model with $M \sim 1420$ MeV/c^2 cannot reproduce the experimental data.

The Faddeev method is suitable for treating final-state interactions of three particles. However, it is difficult to apply this method to the present high-energy p-induced processes where so many partial waves are involved. On the other hand, for the low-energy $K^- + d$ reaction Révai [37] succeeded in extracting the $\Lambda(1405)$ resonance structure by using the Faddeev method. We are considering an analysis of future data of stopped K^- on d, proposed in [18,20], by fully taking account of final-state interactions in the Faddeev formalism.

The proton angular distribution in Λ^* production was also calculated. The isotropic distribution observed in HADES [30] and DISTO [33,34] were explained by a short-range collision with an intermediate boson mass heavier than the ρ meson mass. This is consistent with the calculated large cross section for the production of K^-pp in pp collisions [4], which has recently been observed in DISTO experiments [32].

ACKNOWLEDGMENTS

This work is supported by a Grant-in-Aid for Scientific Research from the Ministry of Science, Research, and Technology of Iran and by a Grant-in-Aid for Scientific Research from Monbukagakusho of Japan. One of us (T.Y.) acknowledges support by the Alexander von Humboldt Foundation, Germany.

[1] M. H. Alston *et al.*, Phys. Rev. Lett. **6**, 698 (1961).
[2] R. H. Dalitz and S. F. Tuan, Ann. Phys. (NY) **8**, 100 (1959).
[3] Y. Akaishi and T. Yamazaki, Phys. Rev. C **65**, 044005 (2002).
[4] T. Yamazaki and Y. Akaishi, Phys. Rev. C **76**, 045201 (2007).
[5] Y. Akaishi, K. S. Myint, and T. Yamazaki, Proc. Jpn. Acad. B **84**, 264 (2008).
[6] R. H. Dalitz and A. Deloff, J. Phys. G **17**, 289 (1991).
[7] K. Nakamura *et al.* (Particle Data Group), J. Phys. G **37**, 075021 (2010).

[8] J. Beringer *et al*. (Particle Data Group), Phys. Rev. D **86**, 010001 (2012).
[9] T. Yamazaki and Y. Akaishi, Phys. Lett. B **535**, 70 (2002).
[10] A. Doté, H. Horiuchi, Y. Akaishi, and T. Yamazaki, Phys. Lett. B **590**, 51 (2004).
[11] A. Doté, H. Horiuchi, Y. Akaishi, and T. Yamazaki, Phys. Rev. C **70**, 044313 (2004).
[12] T. Yamazaki, A. Doté, and Y. Akaishi, Phys. Lett. B **587**, 167 (2004).
[13] D. Jido, J. A. Oller, E. Oset, A. Ramos, and U. G. Meissner, Nucl. Phys. A **725**, 181 (2003).
[14] V. K. Magas, E. Oset, and A. Ramos, Phys. Rev. Lett. **95**, 052301 (2005).
[15] T. Hyodo and W. Weise, Phys. Rev. C **77**, 035204 (2008).
[16] A. Doté, T. Hyodo, and W. Weise, Phys. Rev. C **79**, 014003 (2009).
[17] J. Esmaili, Y. Akaishi, and T. Yamazaki, Phys. Lett. B **686**, 23 (2010).
[18] J. Esmaili, Y. Akaishi, and T. Yamazaki, Phys. Rev. C **83**, 055207 (2011).
[19] B. Riley, I-T. Wang, J. G. Fetkovich, and J. M. McKenzie, Phys. Rev. D **11**, 3065 (1975).
[20] T. Suzuki, J. Esmaili, and Y. Akaishi, EPJ Web Conf. **3**, 07014 (2010).
[21] D. Jido, E. Oset, and T. Sekihara, Eur. Phys. J. A **42**, 257 (2009).
[22] K. Miyagawa and J. Haidenbauer, Phys. Rev. C **85**, 065201 (2012).
[23] O. Braun *et al*., Nucl. Phys. B **129**, 1 (1977).
[24] J-PARC E31 experiment, http://j-parc.jp/researcher/Hadron/en/pac_0907/pdf/Noumi.pdf.
[25] I. Zychor *et al*., Phys. Lett. B **660**, 167 (2008).
[26] L. S. Geng and E. Oset, Eur. Phys. J. A **34**, 405 (2007).
[27] R. J. Hemingway, Nucl Phys. B **253**, 742 (1985).
[28] Y. Akaishi, T. Yamazaki, M. Obu, and M. Wada, Nucl. Phys. A **835**, 67 (2010).
[29] G. Agakishiev *et al*. (HADES Collaboration), Phys. Rev. C **85**, 035203 (2012).
[30] G. Agakishiev *et al*. (HADES Collaboration), Phys. Rev. C **87**, 025201 (2013).
[31] H. Feshbach, Ann. Phys. (NY) **5**, 357 (1958); **19**, 287 (1962).
[32] T. Yamazaki *et al*., Phys. Rev. Lett. **104**, 132502 (2010).
[33] P. Kienle *et al*., Eur. Phys. J. A **48**, 183 (2012).
[34] K. Suzuki *et al*. (private communication).
[35] O. Morimatsu and K. Yazaki, Nucl. Phys. A **483**, 493 (1988).
[36] K. Moriya *et al*., Phys. Rev. C **87**, 035206 (2013).
[37] J. Révai, arXiv:1203.1813v3.